ACS APPLIED MATERIALS & INTERFACES

Research Article

www.acsami.org

Nitrogen-Doped MOF-Derived Micropores Carbon as Immobilizer for Small Sulfur Molecules as a Cathode for Lithium Sulfur Batteries with Excellent Electrochemical Performance

Zhaoqiang Li and Longwei Yin*

Key Laboratory for Liquid−Solid Structural Evolution and Processing of Materials, Ministry of Education, School of Materials Science and Engineering, Shandong University, Jinan 250061, P. R. China

Supporting Information

ABSTRACT: Nitrogen-doped carbon (NDC) spheres with abundant 22 nm mesopores and 0.5 nm micropores are obtained by directly carbonization of nitrogen-contained metal organic framework (MOF) nanocrystals. Large S_8 and small S_{2-4} molecules are successfully infiltrated into 22 nm mesopores and 0.5 nm micropores, respectively. We successfully investigate the effect of sulfur immobilization in mesopores and micropores on the electrochemical performance of lithium−sulfur (Li−S) battery based on NDC−sulfur hybrid cathodes. The large S_8 molecules in 22 nm mesopores can be removed by a prolonged heat treatment, with only small molecules of S_{2-4} immobilized in micropores of NDC matrices. The NDC/S_{2-4} hybrid exhibits excellent cycling performance, high Coulombic efficiency, and good rate capability as cathode for Li−S batteries. The confinement of smaller S_{2-4} molecules in the micropores of NDS efficiently avoids the loss of active sulfur and formation of soluble high-order Li polysulfides. The porous carbon can buffer the volume expansion and contraction changes, promising a stable structure for cathode. Furthermore, N doping in MOF-derived carbon not only facilitates the fast charge transfer but also is helpful in building a stronger interaction between carbon and sulfur, strengthening immobilization ability of S_{2-4} in micropores. The NDS−sulfur hybrid cathode exhibits a reversible capacity of 936.5 mAh g^{-1} at 100th cycle with a Coulombic efficiency of 100% under a current density of 335 mA g^{-1}. It displays a superior rate capability performance, delivering a capacity of 632 mAh g^{-1} at a high rate of 5 A g^{-1}. This uniquely porous NDC derived from MOF nanocrystals could be applied in related high-energy storage devices.

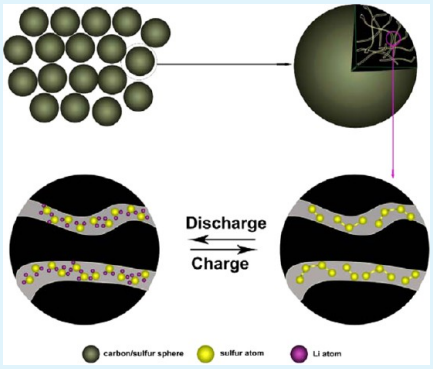

KEYWORDS: *carbon, metal organic framework, nitrogen doping, micropores, lithium sulfur battery*

1. INTRODUCTION

The upgrade of electronic products and electrical vehicles stimulates an intense need for high-energy storage devices.[1,2] Recently, Li−S battery has drawn much attention because sulfur cathode can reach a high theoretical capacity of 1675 mAh g^{-1} and a high-energy density of 2600 Wh kg^{-1}.[3,4] Natural abundance, inexpensiveness, and environmental friendliness of sulfur make Li−S battery one of the most promising energy storage devices.[5] However, several issues need to be solved for sulfur to be used as a cathode for Li−S battery commercial application.[6−9] (i) Sulfur is inherently an electrical insulator, resulting in limited utilization of active material and poor rate capability. (ii) Large volume change (∼80%) during discharge/charge processes leads to the destruction of mechanical integrity and instability of electrochemical performance. (iii) The reaction intermediates of long-chain lithium polysulfides (Li_2S_x, $4 \le x \le 8$) are soluble in electrolyte, causing the loss of active materials during discharge/charge cycles. Furthermore, the polysulfide products may move to and deposit on surface of lithium anode and react with Li metal to form insoluble and insulator lithium sulfides (Li_2S and Li_2S_2) on the surface of Li anode, which may result in a bad contact between Li and electrolyte.[10]

The combination of sulfur with carbon to form a C−S hybrid cathode is efficient to solve these problems. Novel carbon materials with unique structures are promising candidates for immobilizing sulfur as cathode for Li−S batteries because they can improve electron transfer ability, buffer volume change, and effectively retain sulfur. In previous works, combination of sulfur with graphene,[11] carbon nanotubes,[12] and other various carbon materials[13] can effectively improve electrochemical performance. Especially, hierarchically porous carbon monoliths with confined large sulfur content can exhibit a high reversible capacity.[14] Recently, Zheng's study showed that hollow carbon nanofiber-encapsulated sulfur cathodes can deliver a capacity of 730 mAh g^{-1} after 150 cycles,[15] while N-doped porous carbon nanofiber/sulfur as cathode for Li−S battery shows excellent electrochemical performance due to N

Received: November 3, 2014
Accepted: January 27, 2015
Published: January 27, 2015

DOI: 10.1021/am507660y
ACS Appl. Mater. Interfaces 2015, 7, 4029−4038

Scheme 1. Schematic for Synthesis of C−S Hybrids

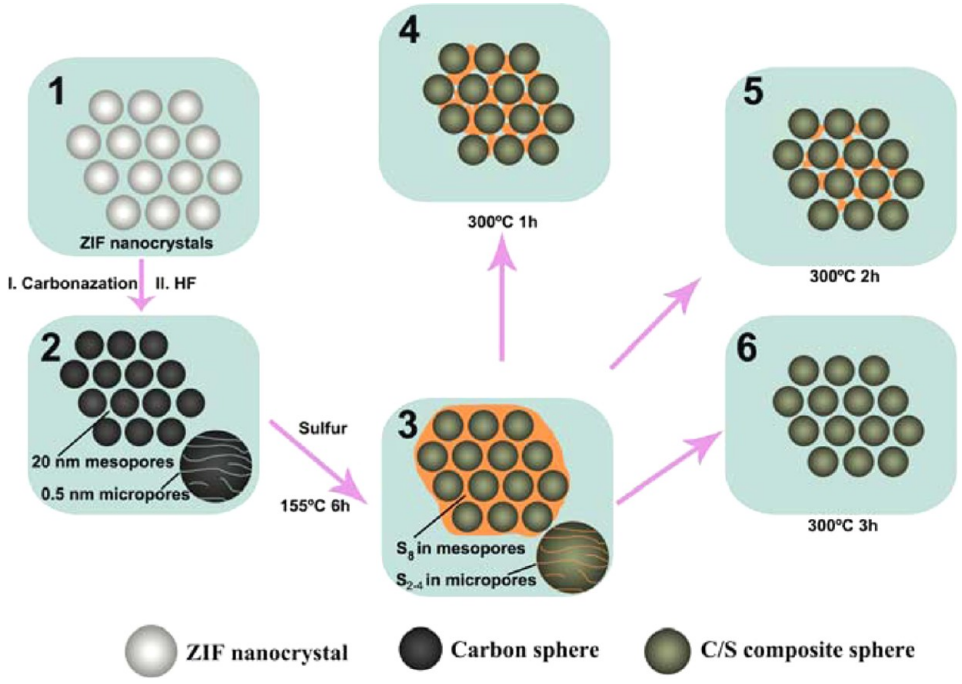

doping.[16] It is revealed that N doping in carbon not only facilitates the fast charge transfer but also is helpful to build a stronger interaction between carbon and sulfur species, strengthening immobilization ability of S and intermediate Li_2S_x.[16−21]

Recently, porous carbon materials obtained by directly carbonization of metal−organic frameworks (MOFs) have drawn much attention due to their large specific surface area, large pore volume, good electrical conductivity, etc. Using a zeolite-type MOF and furfuryl alcohol as precursors, the fabricated porous carbon shows improved H_2 storage capacity due to its exceptional porosity and an unexpectedly high surface area of 3045 $m^2\ g^{-1}$.[22] MOF-derived porous carbon materials could be a promising candidate as a cathode for Li−S batteries.[23] Carbon polyhedrons derived from MOF polyhedrons can be used as a matrix host to incorporate sulfur for Li−S batteries and exhibit stable cycling performance.[24] Because the highly dispersed sulfur in narrow micropores is difficult to release, the microporous carbon/sulfur hybrid cathode can exhibit large reversible capacity and high rate capability.[25,26] Despite previous studies on cathode for Li−S battery, it is highly challenging to effectively immobilize the small sulfur molecules, avoid the loss of active sulfur, and alleviate the dissolution of polysulfides, to realize efficient doping to improve the charge transfer kinetics.

Herein, we for the first time firmly immobilize sulfur components in the form of small sulfur molecules of S_{2-4} within unique 0.5 nm micropores in MOF-derived nitrogen-doped carbon, as a cathode for Li−S battery. The confinement of all small sulfur molecules of S_{2-4} in 0.5 nm micropores avoids the mass loss of active sulfur materials and formation of soluble polysulfides. When acting as cathodes for Li−S batteries, they exhibit high reversible capacity, high Coulombic efficiency, and excellent rate capability. It is believed that the confinement of metastable small S_{2-4} molecules within micropores, N-doping to facilitate charge transfer, and the strain and stress relaxing by the hierarchically mesoporous and microporous structure of MOF-derived carbon, simultaneously make contributions to the excellent electrochemical performance of the Li−S battery.

2. EXPERIMENTAL SECTION

2.1. Synthesis of Zif-8 Nanocrystals, N-Doped Porous Carbon, and Carbon−Sulfur Hybrids. Typically, 2-methylimidazole (Hmim, 98.0%, 6.5 g) was dissolved in 200 mL of methanol to form a transparent solution A. Then a solution of $Zn(NO_3)_2{\cdot}6H_2O$ in methanol was added to form a homogeneous system. Under vigorous stirring at room temperature, the transparent solution turned turbid gradually. After stirring for 1 h, the solution was incubated for 48 h. After centrifugation, washing with methanol several times, and drying at 60 °C overnight, the white Zif-8 products were obtained, and then they were heated at 1000 °C with a heating rate of 5 °C/min for 5 h under Ar flow in a tube furnace. The obtained black powder products were immersed into 20% HF to remove the remaining metal components.

Sulfur and C were thoroughly mixed with a mass ratio of Ms:Mc = 5:1. After that, the mixture was thermally treated under N_2 at 155 °C for 6 h and then treated at 300 °C for different times (1, 2, and 3 h). The obtained samples were denoted as C−S-1, C−S-2 and C−S-3, respectively. During the heating treatment, a slow heating rate of 0.5 °C/min above 115 °C (the melting point of sulfur) helps the sufficient infiltration of sulfur into carbon matrix.

2.2. Materials Characterization. X-ray diffraction (XRD) patterns were obtained using Rigaku D/Max-Rbdiffractometer equipped with Cu Ka radiation (λ = 1.5406 Å). The morphology and chemical components of the synthesized products were analyzed using SU-70 field emission scanning electron microscopy (FESEM) combined with X-ray energy dispersive spectrometry (EDS) and high-resolution transmission electron microscopy (HRTEM) of JEM-2100 at an acceleration voltage of 200 kV. Nitrogen adsorption−desorption isotherms were determined at 77 K using Gold APP VSorb2800P surface area and porosity 60 analyzer. Raman spectra were measured using a 632.8 nm laser with a JY HR800 under ambient conditions, with a laser spot size of about 1 μm. X-ray photoelectron spectroscopy (XPS) characterization was carried out in an ESCALAB 250 instrument with 150W Al Ka probe beam.

2.3. Electrochemical Measurements. The electrochemical measurements were carried out by using 2025 coin-type cells, with C−S hybrid material as working electrode, a celgard 2325 as separator,

DOI: 10.1021/am507660y
ACS Appl. Mater. Interfaces 2015, 7, 4029−4038

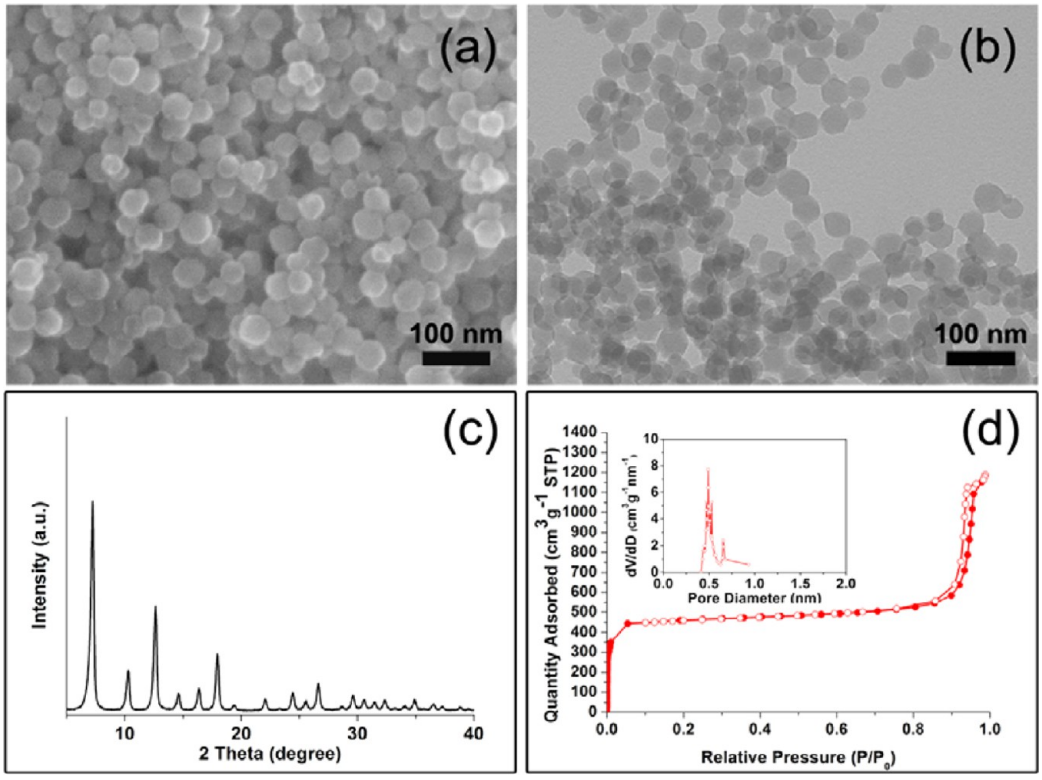

Figure 1. (a) SEM image; (b) TEM image; (c) XRD pattern; (d) nitrogen adsorption−desorption results of ZIF-8 nanocrystals.

a lithium metal foil as reference electrode, and a solution of 1.0 M $LiPF_6$ in mixed EC and DEC (1:1 by volume) as the electrolyte. The electrode consisted of 82 wt % C−S hybrid, 10 wt % ethylene carbonate, and 8 wt % LA-132 (Indigo, China) binder, with a sulfur loading of 1 mg cm^{-2}. The cell were discharged and charged on a battery test system (LAND CT2001A instrument) from 1.0 to 3.0 V at a current density of 335 mA g^{-1}. Cyclic voltammetry (CV) measurements were carried out on an electrochemical workstation (PARSTAT 2273) between 3.0 and 1.0 V at a scan rate of 0.1 mV s^{-1}.

3. RESULTS AND DISCUSSION

Scheme 1 shows the synthesis process of the MOF-derived C−S hybrids. When heated at a high temperature of 1000 °C, the nitrogen-contained Zif-8 nanocrystals can directly transform to N-doped spherical carbon. The Zn-related component can be reduced to metallic Zn and partially evaporate due to its relatively lower boiling point. After further removal of Zn species with HF solution, N-doped carbon spherical products with micropores of 0.5 nm within carbon spheres and mesopores of 22 nm among carbon spheres are obtained. The mixture of sulfur and MOF-derived N-doped carbon was heated at 155 °C; the S_8 ring molecules could break down to small chainlike molecules and penetrate into and be immobilized in the micropores of MOF-derived N-doped carbon. The subsequent 300 °C treatment could evaporate surplus S_8 on the surface and in the mesopores of the C−S hybrids, while the small sulfur molecules cannot easily escape and be stably immobilized in micopores of MOF-derived carbon.

Figure 1 shows SEM, TEM, XRD, and BET results of the synthesized Zif-8 precursors. Zif spherical nanocrystals with a size of 30−40 nm were obtained through the rapid reaction of Zn^{2+} and H-MeIM in methanol (Figure 1a, b). The sharp peak at 7.2° reveals the highly crystalline nature of Zif-8 nanocrystals.[27] All the peaks agree well with that of the XRD patterns of Zif-8 (Figure 1c). As shown in Figure 1d, the Zif-8 nanocrystals exhibit a high surface area of 1486.3 m^2 g^{-1}, a microporous volume of 0.64 cm^3 g^{-1}, and a cumulative pore volume (>2 nm) of 1.21 cm^3 g^{-1}.

FESEM and HRTEM were conducted to study the morphology and microstructure of the MOF-derived samples. As shown in Figure 2a, the MOF-derived N-doped carbon spheres obtained at 1000 °C for 5 h almost maintain the morphology and size of Zif-8 precursors. Due to high surface energy and small size, the N-doped MOF-derived carbons aggregate to form a large amount of mesopores with a pore size of 22 nm, as indicated in the HRTEM image (Figure 2b). Further detailed information on the microstructure of MOF-derived N-doped carbon in Figure 2e reveals abundant disordered micropores within the MOF-derived N-doped carbon. Figure 2c, d depicts FESEM and low-magnification TEM images of sulfur-incorporated MOF-derived N-doped carbon (C−S-3) sample. The higher contrast for C−S-3 hybrid in Figure 2b than for pure C sample results from the sulfur incorporation into the MOF-derived N-doped carbon sample. A HRTEM image in Figure 2f clearly shows the microstructure evolution for the C−S hybrid samples in comparison with pure MOF-derived N-doped carbon sample, indicating that more microporous sites of MOF-derived N-doped carbon are occupied by small sulfur molecules of S_{2-4}. The electron diffraction pattern in Supporting Information Figure S1 suggests an amorphous nature for both carbon and sulfur components.

X-ray diffraction (XRD) patterns of pure sulfur, carbon, and C−S hybrids are depicted in Figure 3a. The sharp diffraction peaks of sublimed sulfur agree well with that of S_8 (PDF No. 83-2283), indicating a highly crystallinity of sulfur precursor. After sulfur was impregnated into MOF-derived N-doped

DOI: 10.1021/am507660y
ACS Appl. Mater. Interfaces 2015, 7, 4029−4038

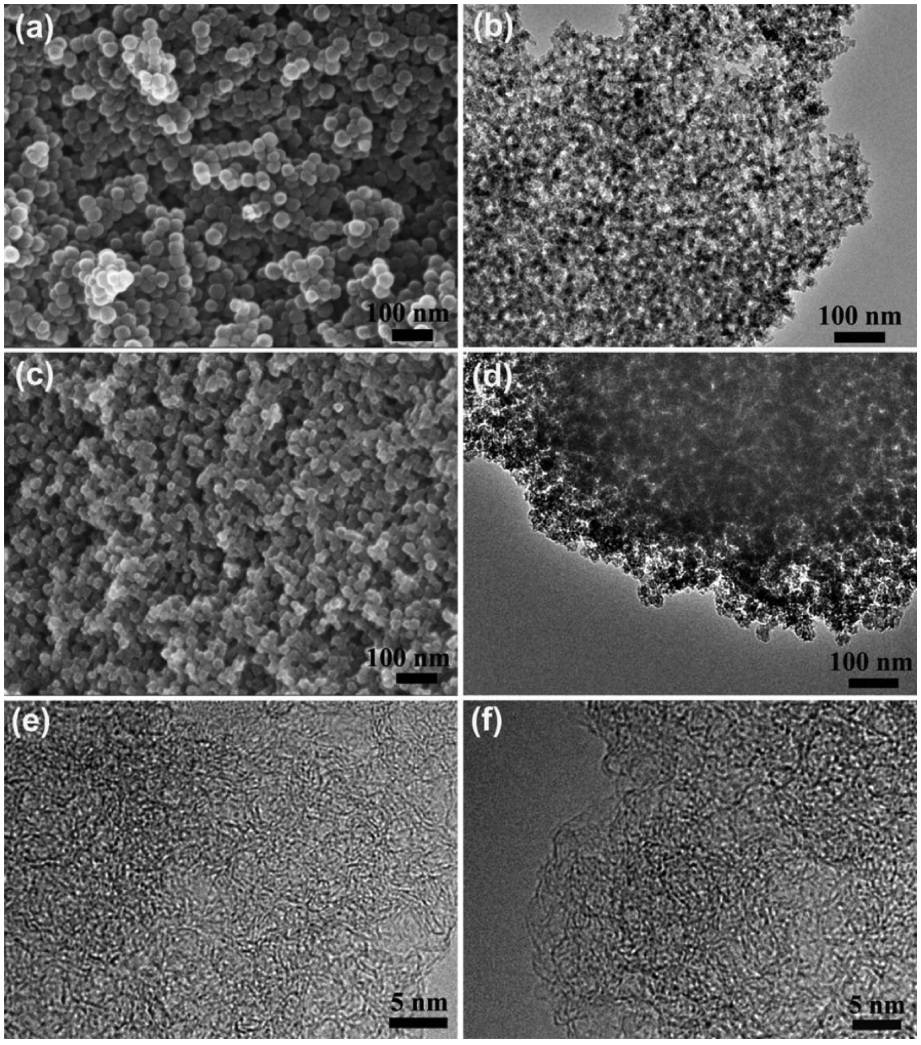

Figure 2. (a, b) SEM, TEM images of MOF-derived nitrogen-doped carbon. (c, d) SEM, TEM images of sulfur incorporated MOF-derived N-doped carbon (C−S-3) sample. (e, f) HRTEM lattice images of MOF-derived N-doped carbon and C−S-3 sample.

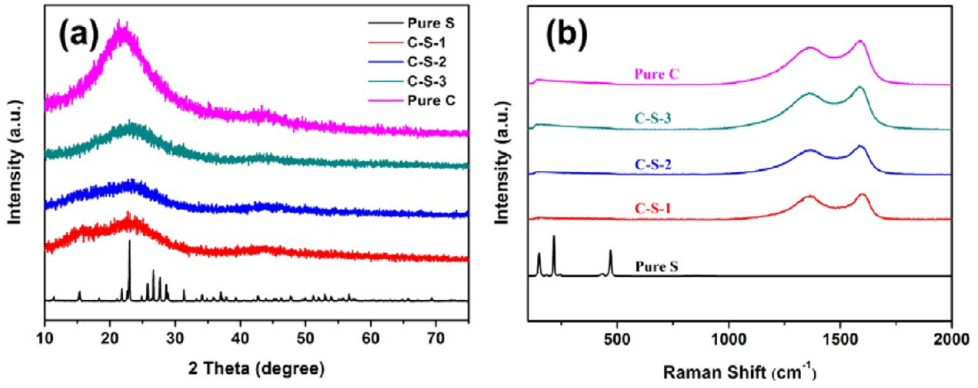

Figure 3. (a) XRD patterns; (b) Raman spectra of pure S and MOF-derived N-doped C and C−S hybrids.

carbon, the sharp diffraction peaks of S_8 disappear completely, indicating an amorphous state for sulfur in the C−S hybrids. The broad diffraction peak at around 24° is associated with partially graphitized carbon in the MOF-derived N-doped carbon samples. In Raman spectra (Figure 3b), the MOF-derived N-doped carbon shows a typical spectrum of partially graphitized carbon, indicated by the G band (1580 cm^{-1}) and D band (1350 cm^{-1}). The G band features the in-plane tangential stretch vibration mode of graphitic layer, and the D band corresponds to the breaking symmetry originating from defects and disorders. The coexistence of G band and D band indicates the partially graphitized nature of the MOF-derived N-doped carbon.[15,28] The sublimed pure sulfur exhibits several peaks below 500 cm^{-1}. However, no characteristic peak is observed in the C−S hybrids, revealing a smaller size and amorphous state for sulfur in MOF-derived N-doped C−S

DOI: 10.1021/am507660y
ACS Appl. Mater. Interfaces 2015, 7, 4029−4038

hybrids. Sulfur is believed to be amorphously impregnated into micropores of N-doped MOF-derived C samples.[25,26]

The nitrogen adsorption−desorption isotherms and pore size distribution curves are shown in Figure 4. For the MOF-derived

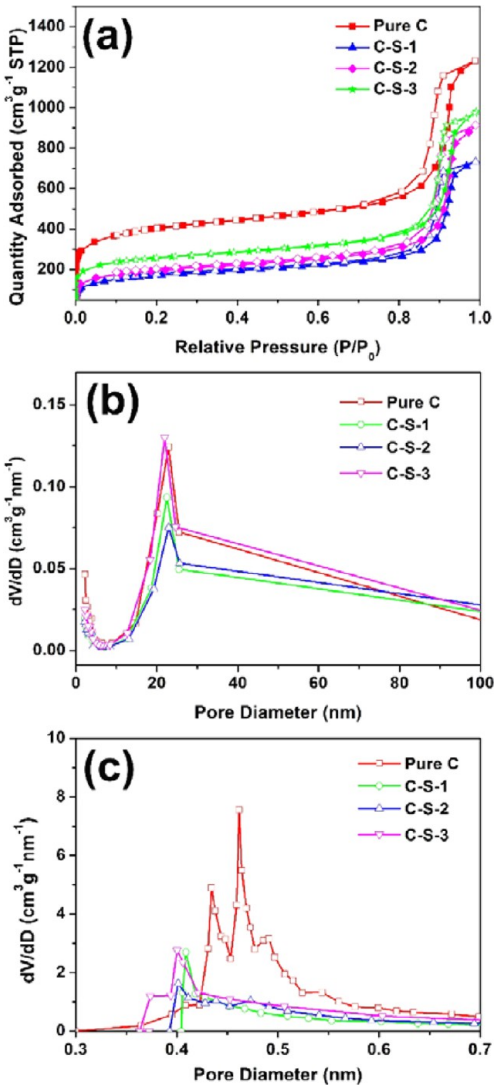

Figure 4. (a) N_2 adsorption−desorption isotherms, (b) mesopore (>2 nm) size distribution, and (c) micropore size distribution of MOF-derived N-doped C and C−S hybrids.

N-doped C sample, the approximately vertical rise of the isotherm at low-pressure range ($P/P_0 \sim 0$) reveals the presence of a large amount of micropores. The hysteresis loop at P/P_0 of 0.8−0.95 can be due to the presence of mesopores.[29] It shows that two types of pores are contained in the S−C hybrids. One type is mesopore with a narrow pore size distribution of about 22 nm (Figure 4b by BJH method); the other type is micropore with a size of 0.5 nm (Figure 4c by HK method). The MOF-derived N-doped C exhibits a high specific surface area of 1104.5 $m^2\ g^{-1}$, a mesoporous volume of 1.14 $cm^3\ g^{-1}$, and microporous volume of 0.39 $cm^3\ g^{-1}$. The specific surface areas of C−S hybrids decrease to 252.6, 307.9, and 438.6 $m^2\ g^{-1}$ for C−S-1, C−S-2, and C−S-3 samples, respectively. Due to the impregnation of sulfur, a large amount of pores have been occupied, thus leading to obvious decrease of the specific surface area. From Table 1, it is shown that the average pore

Table 1. Textural Parameters of MOF-Derived N-Doped C and C−S Hybrids

sample	BET surface area ($m^2\ g^{-1}$)	pore diameter (nm)	pore (>2 nm) volume ($cm^3\ g^{-1}$)	micropore volume ($cm^3\ g^{-1}$)
pure C	1104.5	16.79	1.14	0.39
C−S-1	252.6	18.58	0.81	0.03
C−S-2	307.9	18.92	0.94	0.04
C−S-3	438.6	19.36	1.12	0.05

diameter of C is smaller than that of C−S composites. The reason for a larger pore diameter of C−S composite than that of C sample is that a large amount of sulfur molecules are confined in micropores, resulting in the increase of the average pore diameter of the C−S composites. For the C−S composites, with the treatment time prolonging at a temperature of 300 °C, more and more sulfur molecules evaporate and escape from pores, thus leading to an increase of average pore diameter for the C−S composites, from 18.58 nm for C−S-1 composite, to 18.92 nm for C−S-2 composite, and to 19.36 nm for C−S-3 composite, respectively.

The obtained samples treated at 300 °C for different time of 1, 2, and 3 h are denoted as C−S-1, C−S-2, and C−S-3, respectively. It is interesting to note that with the 300 °C treatment time increasing, more and more sulfur in mesopores and on the surface of C−S hybrids gets evaporated. After 3 h treatment, the mesoporous volume of C−S-3 hybrid is almost the same as that of MOF-derived N-doped carbon, and the microporous volume almost decreases to zero, indicating only small surplus molecules of S_{2-4} are stably immobilized in micopores of MOF-derived N-doped carbon. A decrease in mesoporous (>2 nm) volume observed for the C−S samples indicates the loading of sulfur into the sites of 22 nm mesopores. It is interesting to note that a longer time of heat treatment at 300 °C causes again increase in the mesoporous volume (>2 nm), suggesting the evaporation of sulfur in mesoporous sites. For C−S-3 sample treated at 300 °C for 3 h, the mesoporous volume (>2 nm) is 1.12 $cm^3\ g^{-1}$, approximately the same as that of MOF-derived N-doped C (1.14 $cm^3\ g^{-1}$), indicating the nearly total evaporation of sulfur in mesopores. Compared with MOF N-doped pure C, the microporous volume of the C−S hybrids exhibits a greatly decreasing trend, from 0.39 $cm^3\ g^{-1}$ to 0.03, 0.04, and 0.05 $cm^3\ g^{-1}$, respectively, indicating the firm impregnating of sulfur into micropores. Owing to the space confinement of 0.5 nm micropores, the S_{5-8} molecules cannot exist because of their larger size than 0.5 nm.[26] So it is rationally believed that sulfur exists as small molecules of S_{2-4} within the micropores. The presence of smaller S_{2-4} molecules within micropores can avoid the formation of high-order Li polysulfides.[26,30] This can lead to a good electrochemical performance for S−C hybrid as cathode for Li−S batteries. With the heat treatment time being prolonged, the microporous volume does not show obvious change, revealing the good stability of sulfur in the micropores of MOF-derived N-doped C samples.

The TGA analysis was conducted to confirm the incorporated content of sulfur in the C−S hybrids. As shown in Supporting Information Figure S2, about 37 wt % sulfur was loaded in the C−S-1 sample. After one additional hour's heating treatment at 300 °C, the C−S-2 sample maintains 30 wt % sulfur in the S−C hybrid, indicating further evaporation of sulfur on the surface and in the mesopores. As shown in Supporting Information Figure S2, the sulfur content of the C−

DOI: 10.1021/am507660y
ACS Appl. Mater. Interfaces 2015, 7, 4029−4038

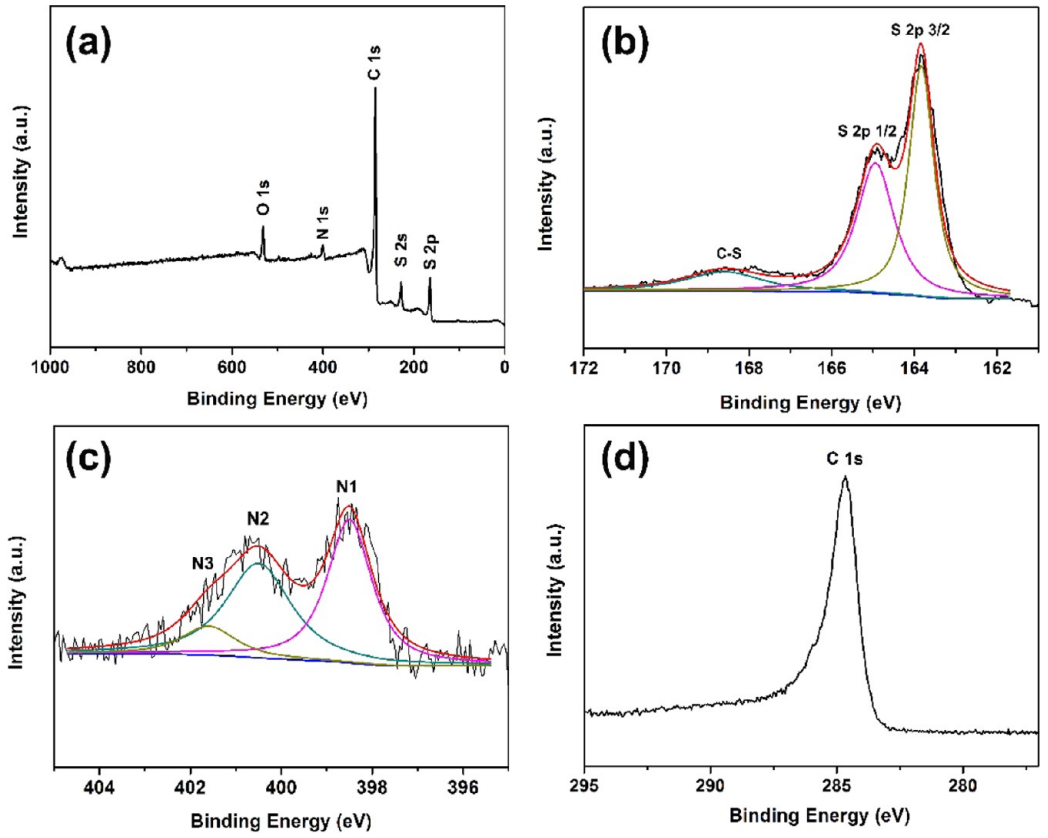

Figure 5. (a) Overall XPS spectrum of C−S-3 hybrid and XPS spectra of (b) S 2p, (c) N 1s, and (d) C 1s.

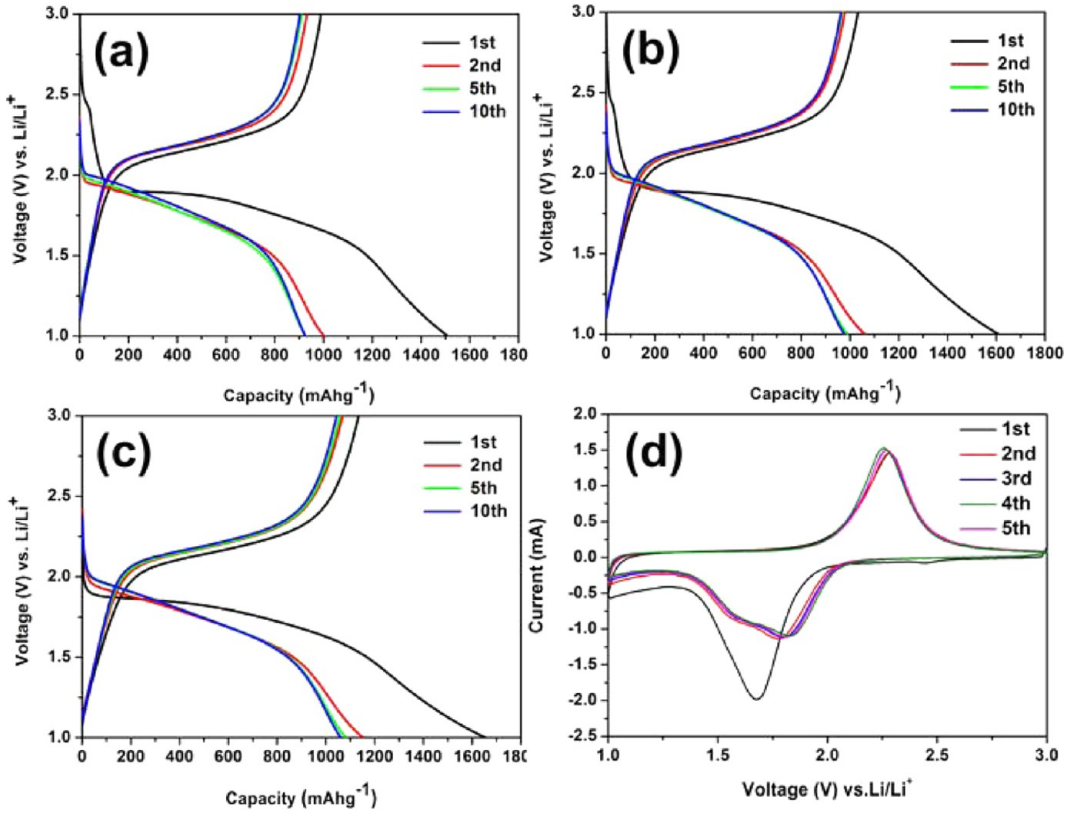

Figure 6. Discharge−charge profiles of (a) C−S-1, (b) C−S-2, and (c) C−S-3 electrodes at a current density of 335 mA g^{-1} in a voltage range 3−1 V. (d) CV curves of C−S-3 electrode for five cycles at a scan rate of 0.1 mV s^{-1} in a voltage range of 3−1 V.

DOI: 10.1021/am507660y
ACS Appl. Mater. Interfaces 2015, 7, 4029−4038

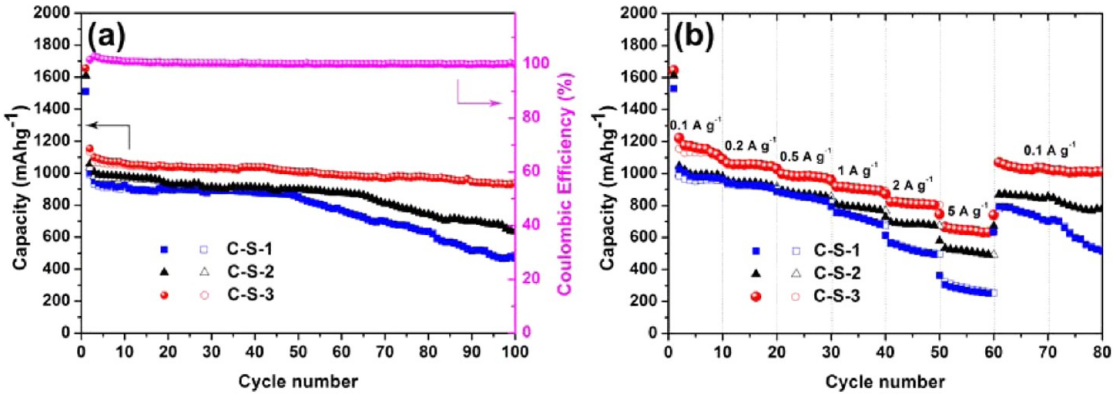

Figure 7. (a) Cycling performance of C−S hybrids at 335 mA g^{-1} (pink circles show the Coulombic efficiency of C−S-3 hybrid sample). (b) Rate capability performance of C−S hybrids.

S-3 sample is 27%, only 3% percent less than that of C−S-2 sample. It is known to all that sulfur in large mesopores and on the surface can easily evaporate at high temperature of 300 °C. So the little difference of sulfur content between C−S-2 and C−S-3 indicates that all the sulfur on the surface and in the mesopores almost evaporates completely after a long heating treatment of 3 h at 300 °C. So C−S-3 sample with almost all the sulfur in the form of smaller molecule of S_{2-4} firmly immobilized in the micropores is expected to exhibit stable electrochemical performance.

Figure 5 shows the XPS spectra of the C−S-3 sample. In the survey spectrum (Figure 5a), five peaks located at 163.8, 228.2, 284.7, 400.0, and 532.0 eV can be easily observed, corresponding to S 2p, S 2s, C 1s, N 1s, and O 1s, respectively. The percentage of N in the sample is high as 5.55 wt % in the C−S-3 hybrid. The N 1s spectrum is fitted into three peaks at 398.5 ± 0.3, 400.5 ± 0.3, and 401.6 ± 0.3 eV, corresponding to pyridinic N (N_1), pyrrolic N (N_2), and graphitic (N_3), respectively. It is previously reported that N_1 atoms are located at the edges of the graphitic carbon layer by replacing C atom of C_6 ring,[31] and N_2 atoms are in the five-membered ring,[32] which can both improve the surface adsorption toward sulfur and polysulfide species. N_3 atoms are doped inside the graphitic carbon plane, thus improving the electrical conductivity of carbon.[16,33] In the S 2p spectra, the two fitted peaks located at 164.8 and 163.6 eV are assigned to S $2p_{1/2}$ and $2p_{3/2}$ due to spin orbit coupling. The fitted S $2p_{3/2}$ has a binding energy of 163.6 eV, which is slightly lower than that of elemental sulfur, indicating the possible presence of C−S chemical bond.[34−36] Furthermore, the presence of the broad high binding energy peak positioned between 167 and 172 eV is direct evidence of the strong chemical interaction between sulfur and carbon.[36,37] The sulfur content of C−S-3 is measured to be 27.32 wt %, agreeing well with the result of TGA analysis. EDS mapping for C−S-3 hybrid further shows a homogeneous distribution of S, C, N elements along the whole hybrid samples (Supporting Information Figure S3).

Coin cells using lithium foil as an anode and C−S hybrid as a cathode were assembled to study the electrochemical performance of C−S hybrids. The charge and discharge voltage profiles of C−S hybrids at a current density of 335 mA g^{-1} (0.2 C) are presented in Figure 6. As shown in Figure 6a, C−S-1 cathode exhibits a short plateau at 2.45 V in the initial discharge process, which may be due to the transformation of S_8 to high-order Li polysulfides.[38] This short plateau disappears in subsequent cycles, indicating the absence of high-order polysulfides due to the consumption by their dissolution and side reaction with carbonate solvent. This is the main reason for the large irreversible capacity. Similarly, the 2.45 V plateau is also observed in the initial discharge process of C−S-2 sample (Figure 6b), but it is shorter than that of C−S-1, indicating a less amount of S_8 molecules in the C−S-2 hybrid. However, this plateau disappears for the C−S-3 cathode (Figure 6c), demonstrating the absence of S_8 molecules in C−S-3 hybrid. This result corresponds well with nitrogen adsorption/desorption results. In the subsequent discharge processes, all the C−S hybrids exhibit a relatively lower discharge plateau (1.82 V) than the ordinary S_8/C cathode. This phenomenon is also reported in previous works[36,39,40] and may be ascribed to the chemical interaction between S and carbon matrix. For the C−S-1 sample, the initial discharge capacity is 1509.4 mAh g^{-1}, with an initial charge capacity of 990.4 mAh g^{-1}. The large irreversible capacity is due to the existence of S_8 in the 22 nm mesopores, which disappears due to the formation of soluble high-order Li polysulfides and side reaction between high-order polysulfides and carbonate solvent. However, C−S-3 cathode exhibits a higher initial discharge capacity of 1658.5 mAh g^{-1}, showing a sufficient reaction of highly dispersed small sulfur molecules in micropores. For all the three C−S hybrids, they exhibit a high Coulombic efficiency and stable capacity in the subsequent cycles, indicating a high stability of small sulfur molecules during discharge/charge processes.

The cyclic voltammograms (CV) of C−S-3 electrode at a scan rate of 0.1 mV s^{-1} are shown in Figure 6d. In the initial cycle, the peak at 1.65 V is due to the formation of insoluble Li_2S and Li_2S_2 from small sulfur molecule of S_{2-4}.[38] In the subsequent cycles, this peak shifts to the position of 1.82 V, and the current of the corresponding peak decreases to a low value.[25] Due to the slow solid-state diffusion kinetics, the solid−solid reduction from insoluble Li_2S_2 to Li_2S is kinetically slow at lower potential region for the bulk sulfur cathode.[40−44] However, owing to the size effect of smaller sized sulfur molecules confined in the micropores, the solid−solid reduction from Li_2S_2 to Li_2S becomes much easier, resulting in the small peak at 1.5−1.6 V. It should be noted that the previously reported cathodic peak at 2.4 V, which is considered to be assigned to the reduction of S_8 to high-order Li polysulfides, is not observed for the present MOF-derived N-doped C−S-3 hybrid cathode, suggesting the absence of large molecules of S_8 in the mesopores and micropores of the hybrid. This is because almost all the sulfur materials are immobilized in micropores of MOF-derived N-doped C for C−S-3 sample,

DOI: 10.1021/am507660y
ACS Appl. Mater. Interfaces 2015, 7, 4029−4038

Scheme 2. Discharge and Charge Mechanism of C−S-3 Hybrid Cathode

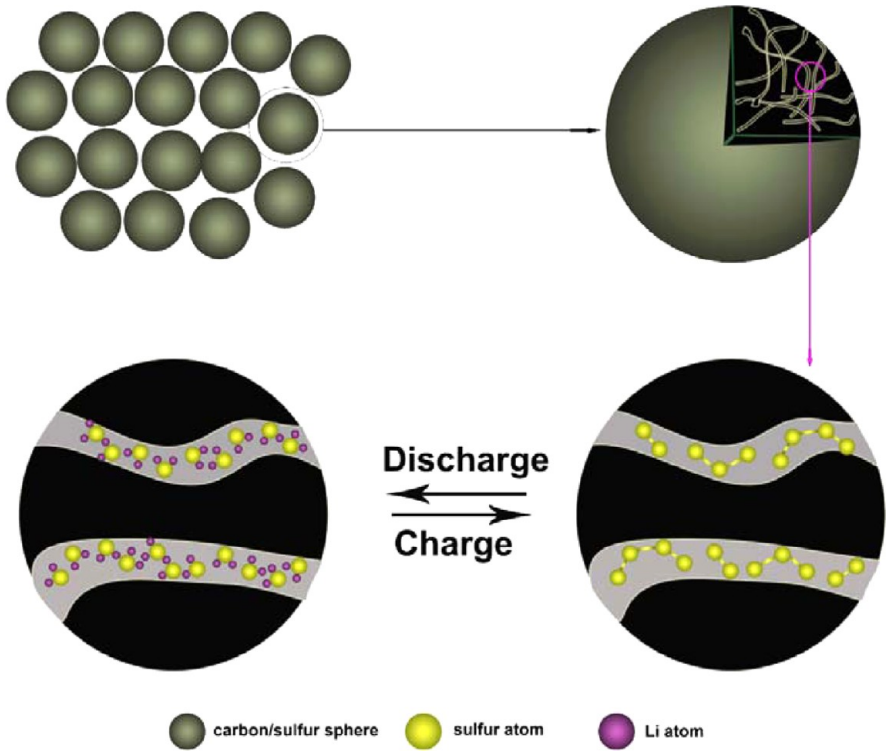

and there is almost no S_8 molecule present, because 3 h treatment at 300 °C makes almost all large sulfur molecules of S_8 get evaporated. On the contrary, it shows an obvious cathodic peak at 2.4 V for C−S-1 sample (see Supporting Information Figure S4) in comparison with that of C−S-3 sample, indicating the presence of large sulfur molecules of S_8 in the mesoporous sites. The peak at 1.5−1.6 V for C−S-1 cathode is due to the transformation from Li_2S_2 to Li_2S. For the initial anodic scan, an oxidation peak is observed at 2.3 V for the C−S-3 hybrid cathode, which can be attributed to the conversion of Li_2S to lithium polysulfide. It is noted that the subsequently anodic curves overlap well with each other, suggesting a good cycling stability of C−S hybrids.

Galvanostatic discharge−charge experiments were carried out to evaluate the lithium storage properties of the C−S samples at a current density of 335 mA g^{-1} in a voltage range of 3−1 V. As shown in Figure 7a, the initial discharge capacity for C−S-1, 2, 3 samples is 1509.4, 1609.1, and 1655.7 mAh g^{-1}, with an initial charge capacity of 990.4, 1033.3, and 1134.2 mAh g^{-1}, respectively. All the C−S hybrid cathodes maintain relatively stable reversible capacity after five discharge/charge cycles. For C−S-1 cathode, it can still exhibit a reversible capacity of 850 mAh g^{-1} at the 50th cycle, with a high Coulombic efficiency of 100.1%. However, the capacity drops gradually in the subsequent cycles, finally only delivering a capacity of 474.3 mAh g^{-1} at the 100th cycle. Similar capacity fading behavior can also be observed in the C−S-2 cathode. This capacity loss should be due to the presence of instable S_8 molecules in the mesopores, and the side reaction production between large polysulfides and carbonate electrolyte may also do harm to the following electrochemical performance. More importantly, the C−S-3 cathode with almost all sulfur molecules in the form of S_{2-4} immobilized in micropores of MOF-derived N-doped carbon exhibits a higher capacity of 1008.7 mAh g^{-1} after 50 cycles, showing a capacity retention of 88% in comparison with the initial capacity. Even after 100 cycles, it can still maintain a specific capacity of 936.5 mAh g^{-1}, demonstrating 82.6% capacity retention in comparison with the initial capacity of the C−S-3 cathode. The results indicate that the C−S-3 hybrid cathodes with small sulfur molecules confined in micropores of MOF-derived N-doped carbon exhibit excellent lithium storage electrochemical activity and cycling stability.

The rate capability of C−S samples is investigated under various current densities from 0.1 to 5 A g^{-1}, as shown in Figure 7b. At the first 30 cycles under relatively low current densities from 0.1 to 0.5 A g^{-1}, all the three C−S hybrid samples display a gradually decreased capacity with the cycle time and current density increasing. At the 30th cycle at a current density of 0.5 A g^{-1}, it shows a reversible capacity of 813.8, 848.2, and 969.6 mAh g^{-1}, respectively, for C−S-1, C−S-2, and C−S-3 samples. However, in comparison with C−S-3 hybrid cathode, after 30 cycles, the capacity of the C−S-1 and C−S-2 hybrid samples decreases faster under higher current densities. The C−S-1 and C−S-2 cathodes show inferior rate capability, displaying a reversible capacity of 251.6, 494.5 mAh g^{-1} at a current density of 5 A g^{-1}, respectively. The C−S-3 hybrid sample can still maintain a reversible capacity of 646.4 mAh g^{-1} after 50 cycles at a current density 5 A g^{-1}. When the current is reduced back to 0.1 A g^{-1}, the capacity recovers back to 910 mAh g^{-1}, indicating a good rate capability of the C−S-3 cathode. Among the C−S hybrids, the C−S-1 contains a relatively larger amount of instable S_8 molecules in the mesopores of the C−S hybrids. For the C−S-3 hybrid, it is shown that almost all sulfur components are stably immobilized in the micropores of the hybrid in the form of smaller molecule of S_{2-4}. EIS tests (Supporting Information Figure S5) show a smaller EIS impedance of C−S-3 electrode, which also promises its better electrochemical performance.

As illustrated in Scheme 2, for C−S-3 hybrid sample, small sulfur molecules are confined in 0.5 nm micropores of MOF-

DOI: 10.1021/am507660y
ACS Appl. Mater. Interfaces 2015, 7, 4029−4038

derived N-doped carbon with abundant micropores and mesopores. When acting as cathode for Li−S batteries, C−S-3 cathode exhibits excellent cycling performance, high Coulombic efficiency, and good rate capability. Such good electrochemical performance should be ascribed to the unique microstructure characteristics that benefit the redox reaction and immobilization of active small sulfur molecules of S_{2-4}. (i) First, sulfur exists as small molecules of S_{2-4} due to the space confinement effect of 0.5 nm micropores. The micropores of MOF-derived N-doped porous carbon can effectively trap sulfur and subsequent lithium polysulfides during cycling, avoiding the shuttle reaction, mass loss of the active materials. (ii) The chemical interactions between carbon and sulfur further immobilize S_{2-4} to prevent its loss. (iii) It is shown from nitrogen adsorption−desorption analysis that the portion of the microporous volume is about 1/4 of the general volume and ensures high maximum sulfur loading. (iv) The abundant porous structure, especially the mesopores of MOF-derived N-doped carbon, can efficiently buffer the volume change during the discharging/charging processes, ensuring a stable structure of the C−S hybrid. (v) The N-doping of MOF-derived carbon with improved electrical conductivity provides an efficient conductive network for the C−S hybrid cathode, resulting in an improved charge transfer kinetics at the interface between the electrode and electrolyte.

4. CONCLUSIONS

In summary, we fabricated MOF-derived nitrogen-doped carbon with hierarchically porous micropore and mesopore structures. The presence of a large portion of microporous volume of 0.39 $cm^3\ g^{-1}$ is enough to effectively immobilize large amounts of active sulfur components. Due to the microporous confinement effect, sulfur can be impregnated into the 0.5 nm micropores of MOF-derived N-doped carbon as small sulfur molecules S_{2-4}, avoiding loss of active sulfur and the formation of soluble high-ordered lithium polysulfides intermediates. Nitrogen doping not only improves the interface charge transfer kinetics but also enhances the interaction between carbon and sulfur species. When the carbon−sulfur hybrids act as cathode for Li−S batteries, they display excellent cycling performance, high Coulombic efficiency, and good rate capability, showing a specific capacity of 1008.7 mAh g^{-1} at the 50th cycle, even still maintaining a specific capacity of 936.5 mAh g^{-1} after 100th cycles under a current density of 335 mA g^{-1}, demonstrating 82.6% capacity retention. Even at a high rate of 5 A g^{-1} after 50 cycles, the C−S-3 hybrid still maintains a specific capacity of 632 mAh g^{-1}. This unique synthetic strategy and MOF-derived N-doped carbon could be applied in other high-energy storage devices.

■ ASSOCIATED CONTENT

Supporting Information

Electron diffraction pattern of C−S-3; TGA curves of the C−S hybrids; elemental mapping results of C−S-3; CV curves of the C−S-1 cathode; Nyquist plots of C−S hybrid electrodes. This material is available free of charge via the Internet at http://pubs.acs.org.

■ AUTHOR INFORMATION

Corresponding Author

*Tel.: + 86 531 88396970. Fax: + 86 531 88396970. E-mail: yinlw@sdu.edu.cn.

Notes

The authors declare no competing financial interest.

■ ACKNOWLEDGMENTS

We acknowledge support from the National Natural Science Funds for Distinguished Young Scholars (No.: 51025211), National Nature Science Foundation of China (No.:51472148, 51272137), and the Tai Shan Scholar Foundation of Shandong Province.

■ REFERENCES

(1) Thackeray, M. M.; Wolverton, C.; Isaacs, E. D. Electrical Energy Storage for Transportation—Approaching the Limits of, and Going Beyond, Lithium-Ion Batteries. *Energy Environ. Sci.* **2012**, *5*, 7854−7863.

(2) Shakoor, R. A.; Kim, H.; Cho, W.; Lim, S. Y.; Song, H.; Lee, J. W.; Kang, J. K.; Kim, Y. T.; Jung, Y.; Choi, J. W. Site-Specific Transition Metal Occupation in Multicomponent Pyrophosphate for Improved Electrochemical and Thermal Properties in Lithium Battery Cathodes: A Combined Experimental and Theoretical Study. *J. Am. Chem. Soc.* **2012**, *134*, 11740−11748.

(3) Dharmasena, P.; Stuart, L. A Solid Sulfur Cathode for Aqueous Batteries. *Science* **1993**, *261*, 1029−1032.

(4) Liang, C.; Dudney, N. J.; Howe, J. Y. Hierarchically Structured Sulfur/Carbon Nanocomposite Material for High-Energy Lithium Battery. *Chem. Mater.* **2009**, *21*, 4724−4730.

(5) Li, D.; Han, F.; Wang, S.; Cheng, F.; Sun, Q.; Li, W. C. High Sulfur Loading Cathodes Fabricated Using Peapodlike, Large Pore Volume Mesoporous Carbon for Lithium−Sulfur Battery. *ACS Appl. Mater. Interfaces* **2013**, *5*, 2208−2213.

(6) Cheon, S.-E.; Ko, K.-S.; Cho, J.-H.; Kim, S.-W.; Chin, E.-Y.; Kim, H.-T. Rechargeable Lithium Sulfur Battery. *J. Electrochem. Soc.* **2003**, *150*, A796−A799.

(7) Yin, L.; Wang, J.; Lin, F.; Yang, J.; Nuli, Y. Polyacrylonitrile/Graphene Composite as a Precursor to a Sulfur-Based Cathode Material for High-Rate Rechargeable Li−S Batteries. *Energy Environ. Sci.* **2012**, *5*, 6966−6972.

(8) Yang, Y.; Zheng, G.; Misra, S.; Nelson, J.; Toney, M. F.; Cui, Y. High-Capacity Micrometer-Sized Li_2S Particles as Cathode Materials for Advanced Rechargeable Lithium-Ion Batteries. *J. Am. Chem. Soc.* **2012**, *134*, 15387−15394.

(9) Elazari, R.; Salitra, G.; Talyosef, Y.; Grinblat, J.; Scordilis-Kelley, C.; Xiao, A.; Affinito, J.; Aurbach, D. Morphological and Structural Studies of Composite Sulfur Electrodes upon Cycling by HRTEM, AFM, and Raman Spectroscopy. *J. Electrochem. Soc.* **2010**, *157*, A1131−A1138.

(10) Shim, J.; Striebel, K. A.; Cairns, E. J. The Lithium/Sulfur Rechargeable Cell. *J. Electrochem. Soc.* **2002**, *149*, A1321−A1325.

(11) Wang, H.; Yang, Y.; Liang, Y.; Robinson, J. T.; Li, Y.; Jackson, A.; Cui, Y.; Dai, H. Graphene-Wrapped Sulfur Particles as a Rechargeable Lithium−Sulfur Battery Cathode Material with High Capacity and Cycling Stability. *Nano Lett.* **2011**, *11*, 2644−2647.

(12) Guo, J.; Xu, Y.; Wang, C. Sulfur-Impregnated Disordered Carbon Nanotubes Cathode for Lithium−Sulfur Batteries. *Nano Lett.* **2011**, *11*, 4288−4294.

(13) Zhang, Z.; Li, Z.; Hao, F.; Wang, X.; Li, Q.; Qi, Y.; Fan, R.; Yin, L. 3D Interconnected Porous Carbon Aerogels as Sulfur Immobilizers for Sulfur Impregnation for Lithium−Sulfur Batteries with High Rate Capability and Cycling Stability. *Adv. Funct. Mater.* **2014**, *24*, 2500−2509.

(14) Yu, L.; Brun, N.; Sakaushi, K.; Eckert, J.; Titirici, M. M. Hydrothermal Nanocasting: Synthesis of Hierarchically Porous Carbon Monoliths and Their Application in Lithium−Sulfur Batteries. *Carbon* **2013**, *61*, 245−253.

(15) Zheng, G.; Yang, Y.; Cha, J. J.; Hong, S. S.; Cui, Y. Hollow Carbon Nanofiber-Encapsulated Sulfur Cathodes for High Specific Capacity Rechargeable Lithium Batteries. *Nano Lett.* **2011**, *11*, 4462−4467.

DOI: 10.1021/am507660y
ACS Appl. Mater. Interfaces 2015, 7, 4029−4038

(16) Yang, J.; Xie, J.; Zhou, X.; Zou, Y.; Tang, J.; Wang, S.; Chen, F.; Wang, L. Functionalized N-Doped Porous Carbon Nanofiber Webs for a Lithium−Sulfur Battery with High Capacity and Rate Performance. *J. Phys. Chem. C* **2014**, *118*, 1800−1807.
(17) Sun, X. G.; Wang, X.; Mayes, R. T.; Dai, S. Lithium−Sulfur Batteries Based on Nitrogen-Doped Carbon and an Ionic-Liquid Electrolyte. *ChemSusChem* **2012**, *5*, 2079−2085.
(18) Wang, Z.; Niu, X.; Xiao, J.; Wang, C.; Liu, J.; Gao, F. First Principles Prediction of Nitrogen-Doped Carbon Nanotubes as a High-Performance Cathode for Li−S Batteries. *RSC Adv.* **2013**, *3*, 16775−16780.
(19) Wang, C.; Su, K.; Wan, W.; Guo, H.; Zhou, H.; Chen, J.; Zhang, X.; Huang, Y. High Sulfur Loading Composite Wrapped by 3D Nitrogen-Doped Graphene as a Cathode Material for Lithium−Sulfur Batteries. *J. Mater. Chem. A* **2014**, *2*, 5018−5023.
(20) Qiu, Y.; Li, W.; Zhao, W.; Li, G.; Hou, Y.; Liu, M.; Zhou, L.; Ye, F.; Li, H.; Wei, Z.; Yang, S.; Duan, W.; Ye, Y.; Guo, J.; Zhang, Y. High-Rate, Ultralong Cycle-Life Lithium/Sulfur Batteries Enabled by Nitrogen-Doped Graphene. *Nano Lett.* **2014**, *14*, 4821−4827.
(21) Wang, Z.; Dong, Y.; Li, H.; Zhao, Z.; Wu, H. B.; Hao, C.; Liu, S.; Qiu, J.; Lou, X. W. Enhancing Lithium−Sulphur Battery Performance by Strongly Binding the Discharge Products on Amino-Functionalized Reduced Graphene Oxide. *Nat. Commun.* **2014**, *5*, 5002.
(22) Jiang, H. L.; Liu, B.; Lan, Y. Q.; Kuratani, K.; Akita, T.; Shioyama, H.; Zong, F.; Xu, Q. From Metal−Organic Framework to Nanoporous Carbon: Toward a Very High Surface Area and Hydrogen Uptake. *J. Am. Chem. Soc.* **2011**, *133*, 11854−11857.
(23) Xi, K.; Cao, S.; Peng, X.; Ducati, C.; Kumar, R. V.; Cheetham, A. K. Carbon with Hierarchical Pores from Carbonized Metal−Organic Frameworks for Lithium Sulphur Batteries. *Chem. Commun.* **2013**, *49*, 2192−2194.
(24) Wu, H. B.; Wei, S.; Zhang, L.; Xu, R.; Hng, H. H.; Lou, X. W. Embedding Sulfur in MOF-Derived Microporous Carbon Polyhedrons for Lithium−Sulfur Batteries. *Chem.—Eur. J.* **2013**, *19*, 10804−10808.
(25) Zhang, B.; Qin, X.; Li, G. R.; Gao, X. P. Enhancement of Long Stability of Sulfur Cathode by Encapsulating Sulfur into Micropores of Carbon Spheres. *Energy Environ. Sci.* **2010**, *3*, 1531−1537.
(26) Xin, S.; Gu, L.; Zhao, N. H.; Yin, Y. X.; Zhou, L. J.; Guo, Y. G.; Wan, L. J. Smaller Sulfur Molecules Promise Better Lithium−Sulfur Batteries. *J. Am. Chem. Soc.* **2012**, *134*, 18510−18513.
(27) Tran, U. P. N.; Le, K. K. A.; Phan, N. T. S. Expanding Applications of Metal−Organic Frameworks: Zeolite Imidazolate Framework ZIF-8 as an Efficient Heterogeneous Catalyst for the Knoevenagel Reaction. *ACS Catal.* **2011**, *1*, 120−127.
(28) Lee, B. S.; Son, S. B.; Park, K. M.; Lee, G.; Oh, K. H.; Lee, S. H.; Yu, W. R. Effect of Pores in Hollow Carbon Nanofibers on Their Negative Electrode Properties for a Lithium Rechargeable Battery. *ACS Appl. Mater. Interfaces* **2012**, *4*, 6702−6710.
(29) (a) Li, Z.; Li, B.; Yin, L.; Qi, Y. Prussion Blue-Supported Annealing Chemical Reaction Route Synthesized Double-Shelled Fe_2O_3/Co_3O_4 Hollow Microcubes as Anode Materials for Lithium-Ion Battery. *ACS Appl. Mater. Interfaces* **2014**, *6*, 8098−8107. (b) Li, Q.; Yin, L.; Li, Z.; Wang, X.; Qi, Y.; Ma, J. Copper Doped Hollow Structured Manganese Oxide Mesocrystals with Controlled Phase Structure and Morphology as Anode Materials for Lithium Ion Battery with Improved Electrochemical Performance. *ACS Appl. Mater. Interfaces* **2013**, *5*, 10975−10984. (c) Gao, J.; Lowe, M. A.; Kiya, Y.; Abruña, H. D. Effects of Liquid Electrolytes on the Charge-Discharge Performance of Rechargeable Lithium/Sulfur Batteries: Electrochemical and in-Situ X-ray Absorption Spectroscopic Studies. *J. Phys. Chem. C* **2011**, *115*, 25132−25137.
(30) Gao, J.; Lowe, M. A.; Kiya, Y.; Abruña, H. D. Effects of Liquid Electrolytes on the Charge−Discharge Performance of Rechargeable Lithium/Sulfur Batteries: Electrochemical and in-Situ X-ray Absorption Spectroscopic Studies. *J. Phys. Chem. C* **2011**, *115*, 25132−25137.
(31) Hulicova-Jurcakova, D.; Seredych, M.; Lu, G. Q.; Bandosz, T. J. Combined Effect of Nitrogen- and Oxygen-Containing Functional Groups of Microporous Activated Carbon on its Electrochemical Performance in Supercapacitors. *Adv. Funct. Mater.* **2009**, *19*, 438−447.
(32) Sun, F.; Wang, J.; Chen, H.; Li, W.; Qiao, W.; Long, D.; Ling, L. High Efficiency Immobilization of Sulfur on Nitrogen-Enriched Mesoporous Carbons for Li−S Batteries. *ACS Appl. Mater. Interfaces* **2013**, *5*, 5630−5638.
(33) Seredych, M.; Hulicova-Jurcakova, D.; Lu, G. Q.; Bandosz, T. J. Surface Functional Groups of Carbons and the Effects of Their Chemical Character, Density, and Accessibility to Ions on Electrochemical Performance. *Carbon* **2008**, *46*, 1475−1488.
(34) Zu, C.; Manthiram, A. Hydroxylated Graphene−Sulfur Nanocomposites for High-Rate Lithium−Sulfur Batteries. *Adv. Energy Mater.* **2013**, *3*, 1008−1012.
(35) Zhang, L.; Ji, L.; Glans, P. A.; Zhang, Y.; Zhu, J.; Guo, J. Electronic Structure and Chemical Bonding of a Graphene Oxide−Sulfur Nanocomposite for Use in Superior Performance Lithium−Sulfur Cells. *Phys. Chem. Chem. Phys.* **2012**, *14*, 13670−13675.
(36) Zheng, S.; Han, P.; Han, Z.; Zhang, H.; Tang, Z.; Yang, J. High Performance C/S Composite Cathodes with Conventional Carbonate-Based Electrolytes in Li−S Battery. *Sci. Rep.* **2014**, *4*, 4842.
(37) Yang, Y.; Yu, G.; Cha, J. J.; Wu, H.; Vosgueritchian, M.; Yao, Y.; Bao, Z.; Cui, Y. Improving the Performance of Lithium Sulfur Batteries by Conductive Polymer Coating. *ACS Nano* **2011**, *5*, 9187−9193.
(38) Wang, D. W.; Zhou, G.; Li, F.; Wu, K. H.; Lu, G. Q.; Cheng, H. M.; Gentle, I. R. A Microporous−Mesoporous Carbon with Graphitic Structure for a High-Rate Stable Sulfur Cathode in Carbonate Solvent-Based Li−S Batteries. *Phys. Chem. Chem. Phys.* **2012**, *14*, 8703−8710.
(39) Lai, C.; Gao, X. P.; Zhang, B.; Yan, T. Y.; Zhou, Z. Synthesis and Electrochemical Performance of Sulfur/Highly Porous Carbon Composites. *J. Phys. Chem. C* **2009**, *113*, 4712−4716.
(40) Yang, Y.; Zheng, G.; Cui, Y. Nanostructured Sulfur Cathodes. *Chem. Soc. Rev.* **2013**, *42*, 3018−3032.
(41) Wang, D.-W.; Zeng, Q.; Zhou, G.; Yin, L.; Li, F.; Cheng, H.-M.; Gentle, I. R.; Lu, G. Q. M. Carbon−Sulfur Composites for Li−S Batteries: Status and Prospects. *J. Mater. Chem. A* **2013**, *1*, 9382−9394.
(42) Zhang, S. S. Liquid Electrolyte Lithium/Sulfur Battery: Fundamental Chemistry, Problems, and Solutions. *J. Power Sources* **2013**, *231*, 153−162.
(43) Barghamadi, M.; Kapoor, A.; Wen, C. A Review on Li−S Batteries as a High Efficiency Rechargeable Lithium Battery. *J. Electrochem. Soc.* **2013**, *160*, A1256−A1263.
(44) Moy, D.; Manivannan, A.; Narayanan, S. R. Direct Measurement of Polysulfide Shuttle Current: A Window into Understanding the Performance of Lithium−Sulfur Cells. *J. Electrochem. Soc.* **2014**, *162*, A1−A7.

DOI: 10.1021/am507660y
ACS Appl. Mater. Interfaces 2015, 7, 4029−4038